



ARTICLE

Preparation and Properties of Polyacrylamide/Sodium Alginate Hydrogel and the Effect of Fe³⁺ Adsorption on Its Mechanical Performance

Zheng Cao^{1,2,3,4,*}, Yang Zhang², Keming Luo², Yinqiu Wu², Hongxin Gao², Junfeng Cheng^{2,*}, Chunlin Liu^{2,3}, Guoliang Tao², Qingbao Guan¹ and Lei Zhang⁵

¹Key Laboratory of High Performance Fibers & Products, Ministry of Education, Donghua University, Shanghai, 201620, China

²Jiangsu Key Laboratory of Environmentally Friendly Polymeric Materials, School of Materials Science and Engineering, Jiangsu Collaborative Innovation Center of Photovoltaic Science and Engineering, Changzhou University, Changzhou, 213164, China

³Changzhou University Huaide College, Jingjiang, 214500, China

⁴National Experimental Demonstration Center for Materials Science and Engineering, Changzhou University, Changzhou, 213164, China

⁵Key Laboratory of Optic-Electric Sensing and Analytical Chemistry for Life Science, MOE, College of Chemistry and Molecular Engineering, Qingdao University of Science and Technology, Qingdao, 266042, China

*Corresponding Authors: Zheng Cao. Email: zcao@cczu.edu.cn; Junfeng Cheng. Email: Junfeng@cczu.edu.cn

Received: 30 December 2020 Accepted: 24 February 2021

ABSTRACT

The preparation and application of functional hydrogels based on natural polysaccharides have always been a hot research topic. In this study, using acrylamide (AM) monomer, N, N'-methylene bisacrylamide (MBA) as cross-linking agent, potassium persulfate (K₂S₂O₈) as initiator, in the presence of natural polysaccharide sodium alginate (SA), the PAM/SA hydrogel was prepared by free radical polymerization. Fourier transform infrared spectroscopy (FT-IR), swelling performance tests, scanning electron microscope (SEM), thermogravimetric analysis (TGA), UV-visible spectrophotometer, mechanical property measurements were carried out to analyze the composition, morphology, and performance of the hydrogels. The swelling behavior, dye adsorption performance, and the mechanical properties of PAM/SA hydrogels before and after Fe³⁺ adsorption were studied. The experimental results showed that the introduction of SA with 4.7%, 7.8%, and 10.3% effectively improved the mechanical and dye adsorption properties of PAM composite hydrogels. The adsorption capacity of PAM/4.7%SA and PAM/10.3%SA hydrogels at equilibrium can reach 40.01 and 44.02 mg/g for methylene blue, which is higher than the value 13.58 mg/g of pure PAM hydrogel. The compressive strength of pure PAM hydrogel is 0.124 MPa. When the SA content is 4.7%, 7.8%, and 10.3%, the compressive strength of the PAM/SA hydrogel was corresponding to 0.130 MPa, 0.134 MPa, and 0.152 MPa, respectively. Fe³⁺ was introduced into the PAM/SA hydrogels, and PAM/SA/Fe³⁺ double-network hydrogels with excellent mechanical properties could be prepared by adjusting the SA content (4.7%, 7.8%, and 10.3%), soaking time (1 h, 2 h, 3 h, 4 h, 5 h, 6 h), and Fe³⁺ concentration (4.76%, 7.41%, 9.09%, and 13.04%). Under the same Fe³⁺ concentration of 9.09% and adsorption time of 4 h, the compressive strengths of the PAM/4.7%SA, PAM/7.8%SA, and PAM/10.3%SA hydrogels could reach 0.354 MPa, 0.767 MPa, and 0.778 MPa, respectively.

KEYWORDS

Sodium alginate; acrylamide; hydrogel; dye adsorption; mechanical properties



1 Introduction

With the development of industrial technology, many synthetic dyes have been used in textile, cosmetics, papermaking, and printing and dyeing industries. However, due to the complex aromatic structure in synthetic dyes, it is difficult to be degraded by organisms. Therefore, the release of dyes in wastewater discharged not only destroys the environment, but also dramatically threatens human health [1–4]. Therefore, the removal of dyes from wastewater is of great significance to environmental protection and human health. Many methods have been adopted for the removal of dyes in water, one of which is photocatalytic degradation [5–9], and the other is adsorption removal [10–12], but the former often requires additional light sources, and the catalyst dispersed in water is difficult to recover. The adsorption method is a crucial application means to remove dyes and other pollutants [13–15].

The hydrogel is a three-dimensional cross-linked network structure system that can maintain its shape even after absorbing a large amount of water [16,17]. Because of the good hydrophilic performance, high water content, excellent biocompatibility, and intelligent response to environmental stimuli (pH [18–20], temperature [21–23], ion intensity [24], near-infrared laser [25,26], and magnetic field [27,28]), the hydrogel has been widely used in catalysis [29–31], biomedical application [32–34], drive and sensor [35–38], drug controlled release [39], energy storage [40–42], wastewater treatment [43], and other fields. For example, Wang et al. [44] reported the preparation of poly (vinyl alcohol)/graphene nanocomposite hydrogel scaffolds and used them for control of cell adhesion. Among many adsorbents, hydrogels have the characteristics of being able to swell in water and simultaneously retain a large amount of water without being dissolved. Hydrogels are easy to introduce functional and charged groups, have a large specific surface area, and have excellent swelling and shrinking properties, effectively removing dye molecules released from the industry [45,46]. Many researchers have done a lot of research work on the preparation, mechanism, and performance of high-strength and high-toughness hydrogels [47–51], but the research on the properties and applications of hydrogel materials still needs further exploration and development.

Generally, polymer hydrogel adsorbents based on polyacrylamide and polyacrylic acid derivatives usually cause secondary environmental pollution after being discarded. Nowadays, many researchers are concerned about applying biomass materials to remove heavy metals and organic pollutants in water, such as chitosan, cellulose, sodium alginate (SA), and other natural polysaccharides [52–58]. These bio-based materials have good biocompatibility, renewability, and degradability, and are promising in various fields [59–62]. Natural polysaccharide polymers such as sodium alginate are cheap and have good compatibility and degradability. Sodium alginate contains many carboxyl groups and hydroxyl groups, so it can exhibit polyanionic behavior in aqueous solutions and has a wide range of applications in the food and pharmaceutical fields [63]. Although sodium alginate is rich in anionic carboxyl groups and has the potential to adsorb cationic dyes, its strong water absorption and solubility in water make it impossible to become a stable adsorbent. Therefore, in this study, sodium alginate and polyacrylamide were used to compound to improve the adsorption and mechanical properties of the hydrogel.

In this study, sodium alginate was introduced into polyacrylamide to prepare PAM/SA hydrogels by free radical polymerization. The composition, morphology, and structure of the PAM/SA hydrogel were characterized by FT-IR, SEM, TGA, etc., and the adsorption property for methylene blue dye, swelling, and mechanical properties of the PAM/SA hydrogel were investigated. Using the ionic cross-linking interaction of the carboxyl group on SA and Fe^{3+} , the PAM/SA- Fe^{3+} double cross-linked network hydrogels with excellent mechanical properties were prepared *in situ* by immersion strategy.

2 Experimental Part

2.1 Chemicals and Materials

Acrylamide (AM), potassium persulfate ($\text{K}_2\text{S}_2\text{O}_8$, 99%), and *N,N'*-methylene bisacrylamide (MBA, 98%) were purchased from Beijing JK Chemical Company, Beijing, China. FeCl_3 , methylene blue,

sodium alginate (SA, chemically pure) were purchased from Shanghai Sinopharm Chemical Reagent Co., Ltd., Shanghai, China. All experimental water is deionized water.

2.2 Preparation of the PAM/SA Hydrogel

First, 0.4 g of $K_2S_2O_8$ was dissolved in 10 mL of deionized water, and 0.5 g of SA was dissolved in 15 mL of deionized water, and the mixture was ultrasonicated until the transparent solution was obtained. 3 mL, 5 mL, and 7 mL of SA solutions were mixed with 7 mL, 5 mL, and 3 mL of AM (2.0 g) aqueous solutions, respectively. Each solution with a volume of 10 mL was ultrasonically shaken to make them thoroughly mixed. Then 0.04 g of MBA and 1 mL of $K_2S_2O_8$ solution (0.4 g/10 mL) were added to the solution obtained above. The mixture was stirred and allowed to react in water bath at 60°C for 8 h. After the reaction was over, the hydrogel was taken out and immersed in the deionized water for removing the unreacted monomers and small residual molecules. The deionized water was changed every 10 h for 3 days. The hydrogel samples were freeze-dried and stored for the following measurements. If the SA content is higher than 10.3%, it cannot be easily dissolved in water, and is not be able to form a uniform transparent solution, resulting in the inhomogeneous hydrogels. Therefore, the SA content was controlled to be 4.7%, 7.8%, and 10.3% for preparing PAM/SA hydrogels. The reference pure PAM hydrogel without adding SA was also prepared according to the procedure mentioned above. The synthetic formula of the hydrogel was shown in Tab. 1. For example, the PAM/SA sample was labeled with “PAM/4.7% SA,” indicating the PAM/SA hydrogel containing 4.7% SA.

Table 1: The recipe for the PAM and PAM/SA hydrogels

Sample	SA (g)	AM (g)	MBA (g)	$K_2S_2O_8$ (g)	H ₂ O (mL)
PAM	–	2.0	–	0.04	10
PAM/4.7%SA	0.10	2.0	0.04	0.04	10
PAM/7.8%SA	0.17	2.0	0.04	0.04	10
PAM/10.3%SA	0.23	2.0	0.04	0.04	10

2.3 Preparation of PAM/SA-Fe³⁺ Hydrogels

The prepared hydrogel samples were soaked into Fe³⁺ solutions with different concentrations (the mass fractions of 4.76%, 7.41%, 9.09%, and 13.04%) for Fe³⁺ adsorption for 1, 2, 3, 4, 5, and 6 h, respectively. After the adsorption of Fe³⁺, the hydrogel sample with Fe³⁺ was freeze-dried and tested for determining the mechanical properties.

2.4 Characterization and Testing of Hydrogels

2.4.1 Mechanical Properties Tests

At room temperature, a universal testing machine was used to test the mechanical properties of the hydrogel, and a mechanical sensor with a maximum load of 1 KN was used. The hydrogel used in the compression test was cylindrical, and the size of the hydrogel was 25 mm in diameter and 23 mm in height. The compression speed of the compressor was set to be 5 mm/min, and the test termination was set to hydrogel fragmentation.

2.4.2 Swelling Behavior Tests

The PAM and PAM/SA hydrogels were freeze-dried to constant weight, and the initial mass (m_0) of the dry hydrogel was accurately weighed. The dry hydrogel sample was soaked into 100 mL of deionized water,

and was swelled at room temperature. At regular intervals, the mass of the hydrogel (m_t) was weighed. The swelling ratio (SR) of the hydrogel was calculated according to Eq. (1).

$$SR = \frac{m_t - m_o}{m_o} \times 100\% \quad (1)$$

2.4.3 SEM Tests

The hydrogel sample was first frozen in liquid nitrogen and then fractured. After the sample section was gold-plated, a JEOL JSM-IT100 scanning electron microscope was used to observe the section's morphology at an accelerating voltage of 10 kV.

2.4.4 FT-IR

The freeze-dried hydrogel samples were tested in the 4000–400 cm^{-1} wave number range using the NICOLET (IS 10) Fourier infrared spectrometer.

2.4.5 Dye Adsorption Tests

First of all, a series of standard solutions of methylene blue were made, and the stock solution was tested by (UV 1800) UV-visible spectroscope to obtain the standard curve. Samples of about 0.01 g were placed in a methylene blue solution for adsorption, and 10 mL is taken out every 10 min for UV visible spectroscopy testing to obtain the adsorption capacity of the dye according to the standard curve.

2.4.6 TGA Analysis

The sample of about 2–3 mg was measured using a 209 F1 Netzsch thermobalance. The heating rate of 20 $^{\circ}\text{C}/\text{min}$, the oxygen atmosphere flow rate of 50 mL/min and the temperature range of 100 $^{\circ}\text{C}$ to 500 $^{\circ}\text{C}$ is set for the measurement.

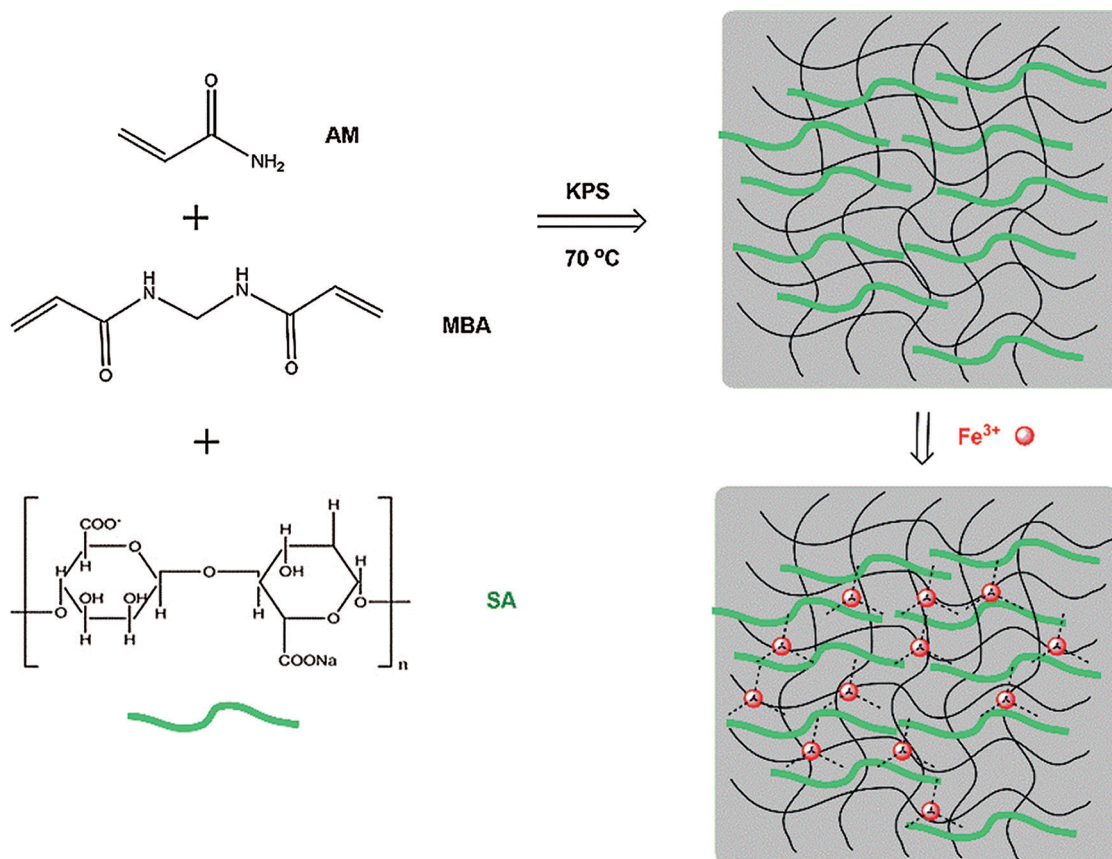
3 Results and Discussion

3.1 Preparation and FT-IR Characterization of PAM/SA Hydrogels

In this study, sodium alginate was introduced into polyacrylamide to prepare hydrogels using free radical polymerization. Using acrylamide as the monomer, potassium persulfate as the initiator, and MBA as the cross-linking agent, upon heating, the initiator potassium persulfate decomposes to generate free radicals and initiates the polymerization of the acrylamide monomer. At the same time, the MBA has a double bond, which can be opened to form a cross-linked polyacrylamide network structure. Sodium alginate exists in the form of linear chains in the solution, eventually forming a semi-interpenetrating cross-linked network structure (as shown in Scheme 1). The swelling behavior, dye adsorption performance, and mechanical properties of the PAM/SA hydrogel have been studied. Since Fe^{3+} can coordinate with carboxylates of SA on the hydrogel network, PAM/SA hydrogels can continue to be cross-linked by Fe^{3+} to form a double cross-linked network structure containing PAM and SA networks.

Fig. 1 shows the FT-IR spectra of PAM, PAM/4.7%SA, PAM/7.8%SA, PAM/10.3%SA, and PAM/4.7%SA/ Fe^{3+} hydrogels. From Fig. 1, it can be seen that the broad peak at 3000–3600 cm^{-1} is attributed to the stretching vibration of O-H, the peak at 2921 cm^{-1} is belonging to the stretching vibration of C-H, and the peaks at around 1618 and 1425 cm^{-1} are assigned to the stretching vibration peak of carboxylate. The absorption peaks at 1035 and 949 cm^{-1} are attributed to C-O stretching vibration and C-O-H deformation vibration [64]. Observing the FT-IR spectra of pure PAM hydrogel, it can be found that the absorption peak at 1641 cm^{-1} belongs to the characteristic stretching vibration of the amide I bond (C=O) [65]. After the addition of SA, it can be seen from the infrared spectra of the prepared PAM/SA hydrogels, because the characteristic absorption peaks of the carboxylate and amide I bond overlap together, resulting in the shift of the absorption peak to a lower wave number position. After soaking in Fe^{3+} solution, the PAM/4.7%SA/ Fe^{3+} hydrogel was obtained. The spectrum of PAM/4.7%SA/ Fe^{3+} hydrogel

was also shown in Fig. 1. From Fig. 1, compared with PAM/SA hydrogels, the PAM/4.7%SA/Fe³⁺ hydrogel shows several new peaks locating at about 1323 and 1118 cm⁻¹, and a broad absorbance band from 500 to 750 cm⁻¹, indicating the presence of inorganic salt and Fe³⁺. It can be seen from the FT-IR results that the PAM/SA hydrogel has been successfully prepared and can be used for the next performance test and characterization.



Scheme 1: Preparation of PAM/SA IPN hydrogel and the formation of double network hydrogels by cross-linking SA chains with Fe³⁺

3.2 Swelling Property of PAM/SA Hydrogels

PAM hydrogel has good water absorption ability due to its hydrophilic amide groups, and SA has strong hydrophilicity due to the -OH and -COOH groups, so in this work, the swelling properties of the hydrogel were investigated and the effect of SA on the swelling properties of PAM hydrogels was verified. Fig. 2 shows the swelling rate of pure PAM and PAM/SA hydrogels as a function of time in deionized water during the swelling test at room temperature. It can be seen from Fig. 2 that the swelling rate of each PAM/SA hydrogel was increased rapidly with the time from 0 to 300 min. Among them, the PAM/SA hydrogel with 10.3% SA shows the fastest swelling rate, while pure PAM hydrogel has the slowest swelling rate. After 300 min, the swelling rate of each hydrogel slowed down, and the pure PAM hydrogel began to reach swelling equilibrium at about 600 min. The PAM/SA hydrogels were continued to swell, and the swelling equilibrium was slowly reached at about 1200 min. It can be observed from Fig. 2 that the swelling rate of the PAM/SA hydrogels synthesized by adding different contents of SA was different when reaching equilibrium. The swelling rate values of PAM and PAM/SA hydrogels

(4.7%, 7.8%, and 10.3%) at the equilibrium are 93.98%, 145.72%, 156.8%, and 171.26%, respectively. This may be because the repulsion of the same negatively charged COO^- groups on the SA linear chain embedded in the networks led to an expanded network structure and more swelling in the deionized water. With the increase of the SA content, the swelling rate of PAM/SA hydrogel was increased. On the other hand, the hydrophilic SA was inserted into the PAM network structure in the form of linear chains. The greater the number of SA linear chains, the greater the obstacle in forming the hydrogel cross-linked structure, and the more likely it is to cause loose semi-interpenetration. Because of the hydrophilic feature of SA in the network, the swelling rate of the PAM/SA hydrogel is greater than that of the pure PAM hydrogel. In summary, the addition of SA can improve the swelling performance of PAM hydrogel.

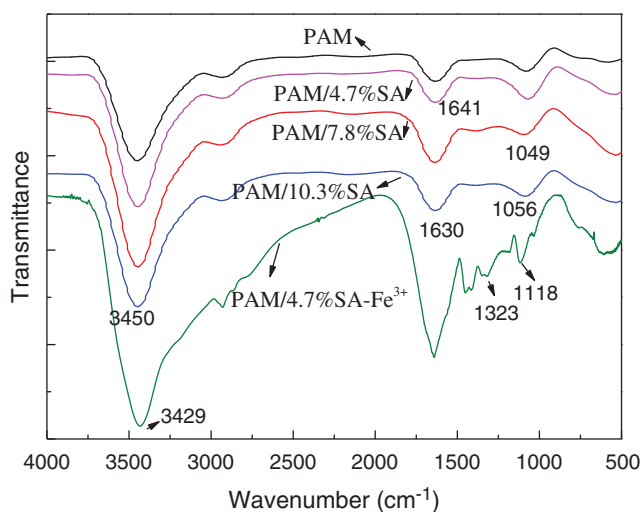


Figure 1: FT-IR spectra of PAM, PAM/4.7%SA, PAM/7.8%SA, PAM/10.3%SA, and PAM/4.7%SA/Fe³⁺ hydrogels

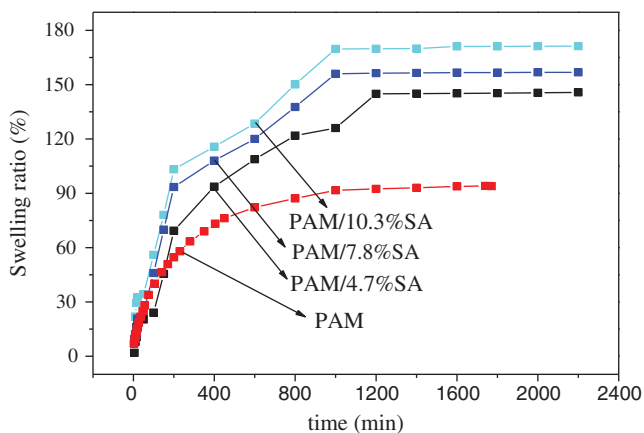


Figure 2: Swelling curves of PAM, PAM/4.7%SA, PAM/7.8%SA, and PAM/10.3%SA hydrogels

3.3 SEM Analysis of PAM/SA Hydrogels

Fig. 3 shows the cross-sectional SEM images of pure PAM hydrogel and PAM/10.3%SA hydrogel. It can be seen from Fig. 3 that the sections of the hydrogel all present a porous structure. However, the PAM hydrogel's pore structure is more compact, and its pore size (19.9 μm) is significantly smaller than

that (39.7 μm) of the PAM hydrogel added with SA. This indicates that the pore size of the PAM hydrogel was increased after SA was added, and the filamentous connections between the pores on the cross-sections of the PAM/SA hydrogel can be clearly observed. Compared to PAM hydrogel, this kind of porous structure may affect the mechanical properties of the PAM/SA hydrogel, which will be analyzed and discussed in the following section.

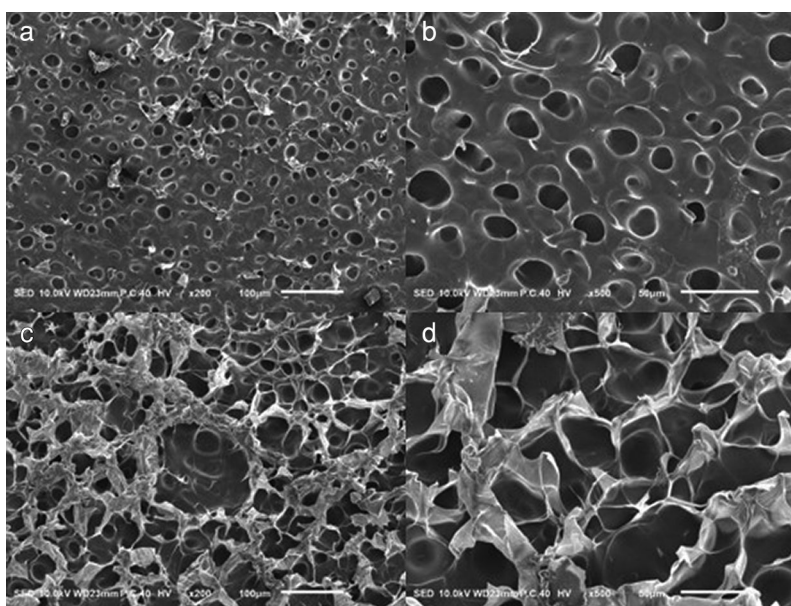


Figure 3: SEM images of pure PAM (a 100 μm , b 50 μm) and PAM/10.3%SA hydrogel (c 100 μm , d 50 μm)

3.4 Dye Adsorption Ability of PAM/SA Hydrogels

SA is rich in anionic carboxyl groups, and the obtained PAM/SA hydrogels can adsorb cationic dyes. Therefore, the adsorption capacity of PAM/SA for cationic methylene blue dyes in this work was also studied. To verify the influence of SA on the dye adsorption performance of PAM hydrogels, dye adsorption tests were performed on the prepared hydrogels, and the adsorption dye selected was methylene blue. The freeze-dried hydrogel with a mass of about 0.01 g was used for the dye adsorption tests. Fig. 4 shows the adsorption capacity of PAM, PAM/4.7%SA, and PAM/10.3%SA hydrogels for methylene blue dyes as a function of time. It can be seen from Fig. 4 that the pure PAM hydrogel also has a small adsorption capacity for methylene blue dye, and the adsorption equilibrium is quickly reached within 60 min. The maximum adsorption capacity of the PAM hydrogel for methylene blue is about 13.58 mg/g. This is mainly due to the van der Waals and hydrogen bonding interactions between the cross-linked PAM network structure and dyes. In contrast, the adsorption capacity of PAM/4.7%SA, PAM/7.8%SA, and PAM/10.3%SA hydrogels at equilibrium can reach 40.01, 42.23, and 44.02 mg/g for methylene blue, which is higher than that of pure PAM hydrogel. This result is mainly due to the electrostatic interaction between the anionic carboxylate on the SA chain and the cationic dye molecules. Therefore, the addition of SA has a positive impact on the adsorption performance of PAM hydrogels. With the increase of SA content, the more effective adsorption sites of the PAM/SA hydrogel for methylene blue, the better the adsorption performance.

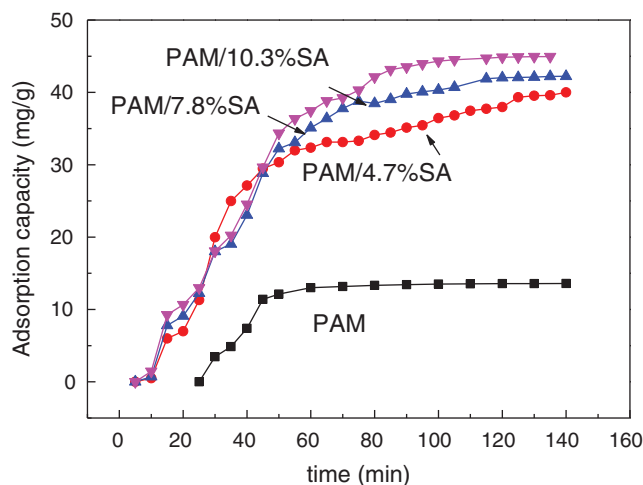


Figure 4: The adsorption capacity of PAM, PAM/4.7%SA, PAM/7.8%SA, and PAM/10.3%SA hydrogels for methylene blue dyes as a function of time

3.5 TGA Analysis of PAM/SA Hydrogels

Fig. 5 shows the TGA and DTG graphs of PAM, PAM/4.7%SA, and PAM/10.3%SA hydrogels. Tab. 2 shows the temperature at different weight-loss rates of PAM, PAM/4.7%SA, and PAM/10.3%SA hydrogels. It can be seen from Fig. 5 and Tab. 2 that when the residual weight fraction is 70%, the degradation temperatures of PAM hydrogel, PAM/4.7%SA, PAM/7.8%SA, and PAM/10.3%SA hydrogel were 321.2, 326.7, 330.1, and 332.9°C, respectively. PAM/10.3%SA hydrogel has the best thermal stability, followed by PAM/7.8%SA, and finally pure PAM hydrogel. The PAM and PAM/SA hydrogel show the same trend when the residual weight fraction is 40%. According to Fig. 5 and Tab. 2, it can be found that the maximum decomposition temperatures of PAM, PAM/4.7%SA, PAM/7.8%SA, and PAM/10.3%SA were 407.0°C, 411.5°C, 416.2°C, and 420.3°C, respectively. That means that adding SA into the PAM hydrogel cross-linked network system can form a semi-interpenetrating polymer network structure and effectively improve the thermal stability of the hydrogel.

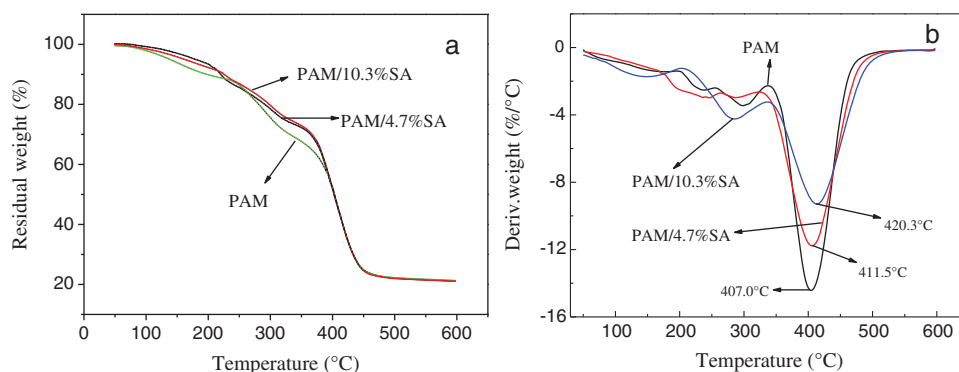


Figure 5: TGA and DTG diagrams of PAM, (a) PAM/4.7%SA, and (b) PAM/10.3%SA hydrogels

Table 2: The degradation temperature of PAM, PAM/4.7%SA, PAM/7.8%SA, and PAM/10.3%SA hydrogels at different weight-loss rates

Samples	Degradation temperature at the residual weight of 70% (°C)	Degradation temperature at the residual weight of 40% (°C)	The maximum degradation peak (°C)
PAM	321.2	401.6	407.0
PAM/4.7%SA	326.7	402.9	411.5
PAM/7.8%SA	330.1	403.8	416.2
PAM/10.3%SA	332.9	405.1	420.3

3.6 Mechanical Properties of PAM/SA Hydrogel before and after Fe^{3+} Adsorption

3.6.1 Mechanical Properties of PAM/SA Hydrogel before Fe^{3+} Adsorption

The next step is to test the mechanical compression properties of PAM/SA hydrogels. Fig. 6 shows the pictures of the visual appearance of Pure PAM, PAM/4.7%SA, PAM/7.8%SA, PAM/10.3%SA hydrogels before and after compression tests (the water content of the hydrogel is about 83%). It can be seen from Fig. 6 that the pure PAM hydrogel was transparent, and the hydrogel was deformed before it was broken in the compression test, so the mechanical properties of the pure PAM hydrogel were poor. Figs. 6b, 6c, and 6d show that the PAM/SA hydrogels were gradually darkened with the increase of SA content, and the degree of breakage of the hydrogels were also increased with the rise in SA content during compression tests. This indicates that the mechanical properties of SA-added PAM hydrogels are different from those of pure PAM hydrogels. Further information can be found from the following analysis on the stress-strain curves.

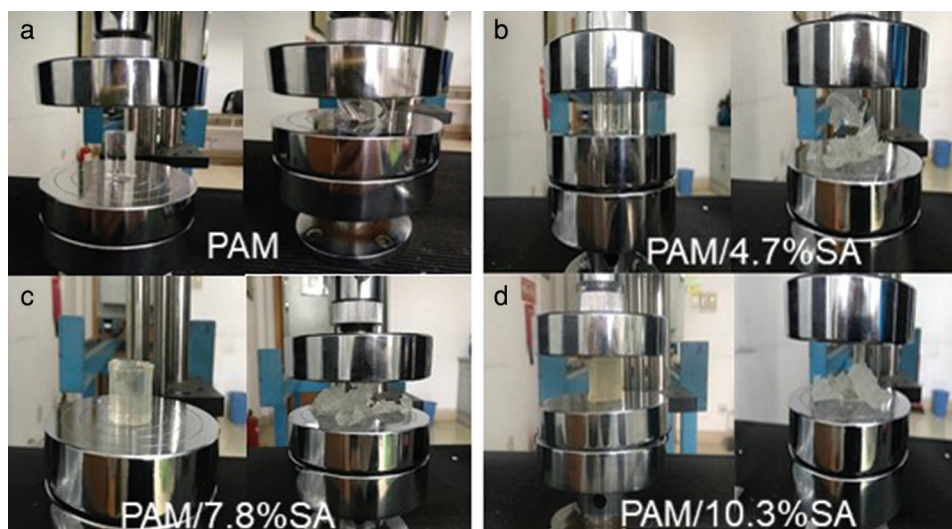
**Figure 6:** The visual appearance of (a) Pure PAM, (b) PAM/4.7%SA, (c) PAM/7.8%SA, (d) PAM/10.3%SA hydrogels before and after compression tests

Fig. 7 shows the stress-strain diagrams of pure PAM, PAM/4.7%SA, PAM/7.8%SA, PAM/10.3%SA hydrogels. During the compression process, it was found that the pure PAM stress-strain curve was above the curves of the PAM composite samples. That is, under the same strain, the stress value of the PAM composite sample is much smaller than that of the PAM pure sample. The pure PAM sample showed more rigidity than PAM composite samples with SA added. The addition of SA has a toughening effect on the

mechanical properties of PAM. The maximum compressive force and compressive strength of each hydrogel sample were obtained in the test. It can be seen from Fig. 7 that the compressive strength of pure PAM hydrogel is 0.124 MPa. When the SA content is 4.7%, 7.8%, and 10.3%, the compressive strength of the PAM/SA hydrogel was corresponding to 0.130 MPa, 0.134 MPa, and 0.152 MPa, respectively. This indicates that the addition of SA can form a semi-interpenetrating cross-linked network structure with the PAM cross-linked network structure. The mechanical strength of the PAM/SA hydrogel was improved as the content of SA increases.

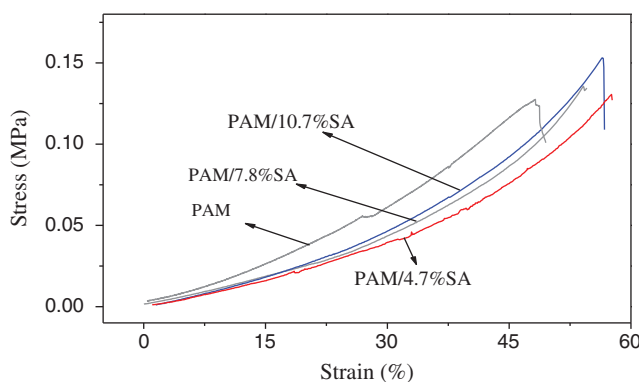


Figure 7: Stress-strain diagrams of pure PAM, PAM/4.7%SA, PAM/7.8%SA, PAM/10.3%SA hydrogels

3.6.2 Mechanical Properties of PAM/SA Hydrogel after Fe^{3+} Adsorption

In order to prepare PAM/SA hydrogels with much stronger mechanical properties, in this research PAM/SA hydrogels were immerse in Fe^{3+} solution, and SA chains were connected to form network structures through the coordination complexation between carboxylate and Fe^{3+} ions. Together with the existing PAM covalent bond network structure, it forms a double cross-linked network structure, which can improve the mechanical properties of the hydrogel. In this study, the influence of SA content, immersion time, and the Fe^{3+} solution concentration on the compressibility of PAM/SA composite hydrogel was investigated. Firstly the effect of different SA content on the compressive strength of PAM and PAM/SA was examined under the same Fe^{3+} concentration and the same adsorption time ($C_{Fe^{3+}} = 9.09\%$, adsorption time is 4 h). Fig. 8 shows the stress-strain diagram of PAM/SA hydrogels with different SA content after Fe^{3+} adsorption. It can be seen from Fig. 8 that the compressive strengths of the PAM/4.7%SA, PAM/7.8%SA, and PAM/10.3%SA hydrogels are 0.354 MPa, 0.767 MPa, and 0.778 MPa, respectively. Compared with the PAM/SA hydrogel without Fe^{3+} , the addition of Fe^{3+} significantly improved the mechanical properties of the PAM/SA hydrogel. In addition, the mechanical properties of the PAM/SA hydrogel soaked in the Fe^{3+} solution with the same concentration for the same time were increased with the increase of SA content. The higher the SA content, the more effective SA sites for complexing and coordination with Fe^{3+} , forming the double cross-linked network structures and improves the mechanical properties.

Then the effect of different Fe^{3+} concentrations on the mechanical properties of PAM/SA hydrogels was studied under the same SA content of 10.3% and the same immersion time of 4 h. In this compression test, the Fe^{3+} concentration was set to be 4.76%, 7.41%, 9.09%, and 13.04%, respectively. Fig. 9 shows the stress-strain diagram of PAM/SA hydrogels after Fe^{3+} adsorption. It can be seen from Fig. 9 that the compression strength of PAM/SA- Fe^{3+} hydrogels immersed in a solution containing 4.76% Fe^{3+} was about 0.495 MPa. As the concentration of the soaked Fe^{3+} solution continued to increase to 13.04%, the mechanical strength of the PAM/SA- Fe^{3+} hydrogel was gradually improved and finally reached 0.820 MPa. It can be concluded from this test that PAM/SA can absorb Fe^{3+} to form an effective double-crosslinked network structure system, and the higher the Fe^{3+} concentration, the more obvious the double-crosslinked network structure is formed, which leads to the enhanced mechanical properties.

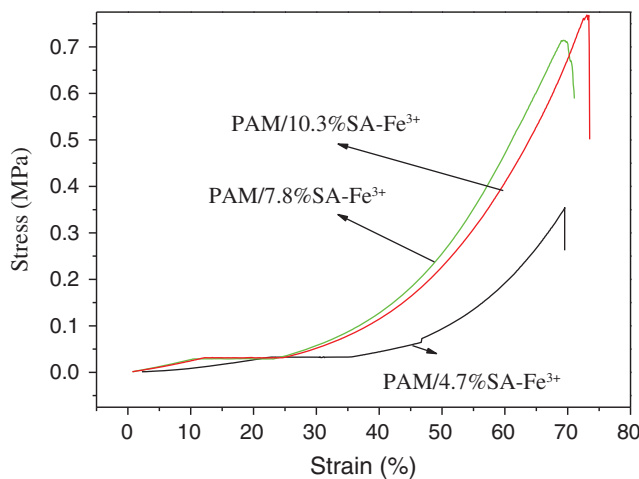


Figure 8: Stress-strain diagram of PAM/SA hydrogels with different SA content after Fe^{3+} adsorption

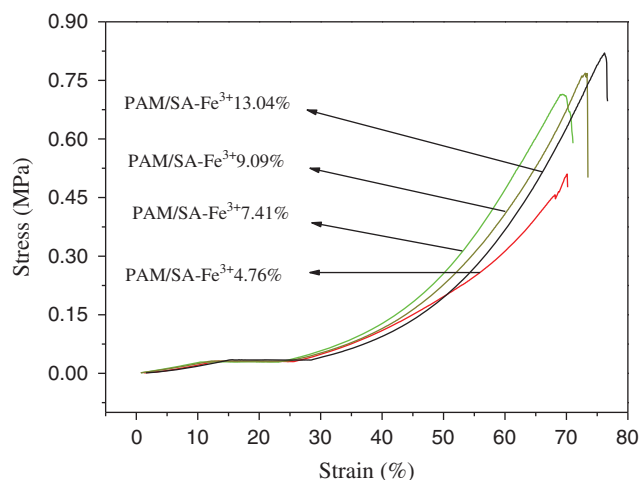


Figure 9: Stress-strain diagram of PAM/SA hydrogels after adsorption of different concentrations of Fe^{3+}

Fig. 10 shows the stress-strain diagram of PAM/SA hydrogel after Fe^{3+} adsorption under different immersion times (SA content is 4.7%, $C_{\text{Fe}^{3+}} = 9.09\%$). The PAM/SA hydrogel has different Fe^{3+} adsorption time, resulting in different mechanical properties of the hydrogel. The compressive strength of the PAM/SA hydrogel with Fe^{3+} adsorbed for 1 h is 0.220 MPa. As the adsorption time increases, the compressive strength of the PAM/SA hydrogel increases. After the PAM/SA hydrogel was immersed in Fe^{3+} solution for 6 h, its strength can reach 0.706 MPa. It can be concluded that the introduction of Fe^{3+} can effectively improve the compression performance of the PAM/SA hydrogel. The longer the Fe^{3+} adsorption time, the more beneficial to the formation of a double-crosslinked network structure and the enhanced mechanical properties.

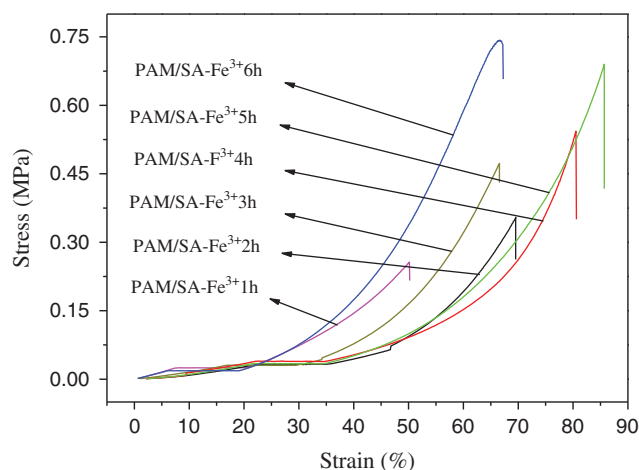


Figure 10: Stress-strain diagram of PAM/SA hydrogel after Fe^{3+} adsorption under different immersion time

4 Conclusion

PAM/SA hydrogels with different SA contents were prepared by free radical polymerization. The addition of SA improved the mechanical properties, swelling properties, and thermal stability of PAM hydrogels. PAM/4.7%SA and PAM/10.3%SA hydrogels have a maximum adsorption capacity of 40.01 and 44.02 mg/g for methylene blue, which is higher than pure PAM hydrogel. This is mainly due to the electrostatic interaction between the anionic carboxylate on the SA chain and the cationic dye molecules. The PAM/SA hydrogel was immersed in Fe^{3+} solution, and the SA chains could be connected to form a network structure through the coordination complexation between carboxylate and iron ions. The effects of different SA content, different immersion time, and different Fe^{3+} solution concentration on the compressibility of PAM/SA hydrogel were studied. The combination of SA networks formed after immersion with the existing PAM network structure leads to forming a double cross-linked network structure, which can improve the mechanical properties of the PAM hydrogel.

Acknowledgement: The authors would like to thank Jinwei Liu from Shiyanjia Lab for support of SEM measurements.

Funding Statement: This project is supported by the National Natural Science Foundation of China (Grant Nos. 21704008, 21644002), Natural Science Foundation of Jiangsu Province, China (Grant No. BK20201449), Natural Science Foundation of the Jiangsu Higher Institutions of China (Grant No. 20KJA430011), Applied Basic Research Project of Changzhou (Grant No. CJ20180052). Financial support provided for this project by the Priority Academic Program Development of Jiangsu Higher Education Institutions (PAPD) and the Top-notch Academic Programs Project of Jiangsu Higher Education Institutions (TAPP), and financial support from the Young Elite Scientist Sponsorship Program of the Jiangsu Province Association of Science and Technology, Postgraduate Research & Practice Innovation Program of Jiangsu Province are also gratefully acknowledged.

Conflicts of Interest: The authors declare that they have no conflicts of interest to report regarding the present study.

References

1. Pearce, C. I., Lloyd, J. R., Guthrie, J. T. (2003). The removal of colour from textile wastewater using whole bacterial cells: A review. *Dyes and Pigments*, 58(3), 179–196. DOI 10.1016/S0143-7208(03)00064-0.

2. Gupta, V. K., Suhas. (2009). Application of low-cost adsorbents for dye removal—A review. *Journal of Environmental Management*, 90(8), 2313–2342. DOI 10.1016/j.jenvman.2008.11.017.
3. Zheng, T., Holford, T. R., Mayne, S. T., Owens, P. H., Boyle, P. et al. (2002). Use of hair colouring products and breast cancer risk: A case-control study in Connecticut. *European Journal of Cancer*, 38(12), 1647–1652. DOI 10.1016/S0959-8049(02)00138-7.
4. Crini, G. (2006). Non-conventional low-cost adsorbents for dye removal: A review. *Bioresource Technology*, 97(9), 1061–1085. DOI 10.1016/j.biortech.2005.05.001.
5. Ajmal, A., Majeed, I., Malik, R. N., Idriss, H., Nadeem, M. A. (2014). Principles and mechanisms of photocatalytic dye degradation on TiO₂ based photocatalysts: A comparative overview. *RSC Advances*, 4(70), 37003–37026. DOI 10.1039/C4RA06658H.
6. Stock, N. L., Peller, J., Vinodgopal, K., Kamat, P. V. (2000). Combinative sonolysis and photocatalysis for textile dye degradation. *Environmental Science & Technology*, 34(9), 1747–1750. DOI 10.1021/es991231c.
7. Chen, J., Xiong, Y., Duan, M., Li, X., Li, J. et al. (2020). Insight into the synergistic effect of adsorption-photocatalysis for the removal of organic dye pollutants by Cr-doped ZnO. *Langmuir*, 36(2), 520–533. DOI 10.1021/acs.langmuir.9b02879.
8. Wen, M., Cheng, M., Zhou, S., Wu, Q., Wang, N. et al. (2012). Synthesis of reusable NiCo@Pt nanoalloys from icosahedrons to spheres by element lithography and their synergistic photocatalysis for Nano-ZnO toward dye wastewater degradation. *Journal of Physical Chemistry C*, 116(21), 11702–11708. DOI 10.1021/jp2115912.
9. Yu, K., Yang, S., Liu, C., Chen, H., Li, H. et al. (2012). Degradation of organic dyes via bismuth silver oxide initiated direct oxidation coupled with sodium bismuthate based visible light photocatalysis. *Environmental Science & Technology*, 46(13), 7318–7326. DOI 10.1021/es3001954.
10. Molavi, H., Hakimian, A., Shojaei, A., Raeiszadeh, M. (2018). Selective dye adsorption by highly water stable metal-organic framework: Long term stability analysis in aqueous media. *Applied Surface Science*, 445, 424–436. DOI 10.1016/j.apsusc.2018.03.189.
11. Li, Y., Du, Q., Liu, T., Peng, X., Wang, J. et al. (2013). Comparative study of methylene blue dye adsorption onto activated carbon, graphene oxide, and carbon nanotubes. *Chemical Engineering Research and Design*, 91(2), 361–368. DOI 10.1016/j.cherd.2012.07.007.
12. Yagub, M. T., Sen, T. K., Afroze, S., Ang, H. M. (2014). Dye and its removal from aqueous solution by adsorption: A review. *Advances in Colloid and Interface Science*, 209(1), 172–184. DOI 10.1016/j.cis.2014.04.002.
13. Rafatullah, M., Sulaiman, O., Hashim, R., Ahmad, A. (2010). Adsorption of methylene blue on low-cost adsorbents: A review. *Journal of Hazardous Materials*, 177(1–3), 70–80. DOI 10.1016/j.jhazmat.2009.12.047.
14. Chen, J., Sheng, Y., Song, Y., Chang, M., Zhang, X. et al. (2018). Multimorphology mesoporous silica nanoparticles for dye adsorption and multicolor luminescence applications. *ACS Sustainable Chemistry & Engineering*, 6(3), 3533–3545. DOI 10.1021/acssuschemeng.7b03849.
15. Mittal, A., Gajbe, V., Mittal, J. (2008). Removal and recovery of hazardous triphenylmethane dye, Methyl Violet through adsorption over granulated waste materials. *Journal of Hazardous Materials*, 150(2), 364–375. DOI 10.1016/j.jhazmat.2007.04.117.
16. Ahmed, E. M. (2015). Hydrogel: Preparation, characterization, and applications: A review. *Journal of Advanced Research*, 6(2), 105–121. DOI 10.1016/j.jare.2013.07.006.
17. Zhang, Y. S., Khademhosseini, A. (2017). Advances in engineering hydrogels. *Science*, 356(6337), eaaf3627. DOI 10.1126/science.aaf3627.
18. Chen, T., Liu, H., Dong, C., An, Y., Liu, J. et al. (2020). Synthesis and characterization of temperature/pH dual sensitive hemicellulose-based hydrogels from eucalyptus APMP waste liquor. *Carbohydrate Polymers*, 247(2), 116717. DOI 10.1016/j.carbpol.2020.116717.
19. Nezami, S., Sadeghi, M., Mohajerani, H. (2020). A novel pH-sensitive and magnetic starch-based nanocomposite hydrogel as a controlled drug delivery system for wound healing. *Polymer Degradation and Stability*, 179(8), 109255. DOI 10.1016/j.polymdegradstab.2020.109255.

20. Gao, J., Xu, Y., Zheng, Y., Wang, X., Li, S. et al. (2019). pH-sensitive carboxymethyl chitosan hydrogels via acid-labile ortho ester linkage as an implantable drug delivery system. *Carbohydrate Polymers*, 225(6), 115237. DOI 10.1016/j.carbpol.2019.115237.
21. Pelton, R. H., Chibante, P. (1986). Preparation of aqueous latices with N-isopropylacrylamide. *Colloids and Surfaces*, 20(3), 247–256. DOI 10.1016/0166-6622(86)80274-8.
22. Saunders, B. R., Vincent, B. (1999). Microgel particles as model colloids: Theory, properties and applications. *Advances in Colloid and Interface Science*, 80(1), 1–25. DOI 10.1016/S0001-8686(98)00071-2.
23. Cao, Z., Du, B., Chen, T., Nie, J., Xu, J. et al. (2008). Preparation and properties of thermo-sensitive organic/inorganic hybrid microgels. *Langmuir*, 24(22), 12771–12778. DOI 10.1021/la802087n.
24. Guo, P., Liang, J., Li, Y., Lu, X., Fu, H. et al. (2019). High-strength and pH-responsive self-healing polyvinyl alcohol/poly 6-acrylamidohexanoic acid hydrogel based on dual physically cross-linked network. *Colloids and Surfaces A: Physicochemical and Engineering Aspects*, 571, 64–71. DOI 10.1016/j.colsurfa.2019.03.027.
25. Cao, Z., Hu, Y., Yu, Q., Lu, Y., Wu, D. et al. (2017). Facile fabrication, structures, and properties of laser-marked polyacrylamide/Bi₂O₃ hydrogels. *Advanced Engineering Materials*, 19, 1600826.
26. Cao, Z., Chen, Y., Zhang, C., Cheng, J., Wu, D. et al. (2019). Preparation of near-infrared laser responsive hydrogels with enhanced laser marking performance. *Soft Matter*, 15(14), 2950–2959. DOI 10.1039/C8SM02635A.
27. Chen, T., Cao, Z., Guo, X., Nie, J., Xu, J. et al. (2011). Preparation and characterization of thermosensitive organic-inorganic hybrid microgels with functional Fe₃O₄ nanoparticles as crosslinker. *Polymer*, 52(1), 172–179. DOI 10.1016/j.polymer.2010.11.014.
28. Wang, Y., Dong, A., Yuan, Z., Chen, D. (2012). Fabrication and characterization of temperature-, pH- and magnetic-field-sensitive organic/inorganic hybrid poly (ethylene glycol)-based hydrogels. *Colloids and Surfaces A: Physicochemical and Engineering Aspects*, 415, 68–76. DOI 10.1016/j.colsurfa.2012.10.009.
29. Godiya, C. B., Sayed, S. M., Xiao, Y., Lu, X. (2020). Highly porous egg white/polyethyleneimine hydrogel for rapid removal of heavy metal ions and catalysis in wastewater. *Reactive and Functional Polymers*, 149(13), 104509. DOI 10.1016/j.reactfunctpolym.2020.104509.
30. Yao, T., Jia, W., Tong, X., Feng, Y., Qi, Y. et al. (2018). One-step preparation of nanobeads-based polypyrrole hydrogel by a reactive-template method and their applications in adsorption and catalysis. *Journal of Colloid and Interface Science*, 527, 214–221. DOI 10.1016/j.jcis.2018.05.052.
31. Sahiner, N., Butun, S., Ozay, O., Dibek, B. (2012). Utilization of smart hydrogel-metal composites as catalysis media. *Journal of Colloid and Interface Science*, 373(1), 122–128. DOI 10.1016/j.jcis.2011.08.080.
32. Zhang, W., Wang, R., Sun, Z., Zhu, X., Zhao, Q. et al. (2020). Catechol-functionalized hydrogels: Biomimetic design, adhesion mechanism, and biomedical applications. *Chemical Society Reviews*, 49(2), 433–464. DOI 10.1039/C9CS00285E.
33. Cui, C., Wu, T., Chen, X., Liu, Y., Li, Y. et al. (2020). A janus hydrogel wet adhesive for internal tissue repair and anti-postoperative adhesion. *Advanced Functional Materials*, 30(49), 2005689. DOI 10.1002/adfm.202005689.
34. Qu, J., Zhao, X., Liang, Y., Zhang, T., Ma, P. X. et al. (2018). Antibacterial adhesive injectable hydrogels with rapid self-healing, extensibility and compressibility as wound dressing for joints skin wound healing. *Biomaterials*, 183, 185–199. DOI 10.1016/j.biomaterials.2018.08.044.
35. Wu, B. Y., Le, X. X., Jian, Y. K., Lu, W., Yang, Z. Y. et al. (2019). pH and thermo dual-responsive fluorescent hydrogel actuator. *Macromolecular Rapid Communications*, 40(4), 1800648. DOI 10.1002/marc.201800648.
36. Ma, C., Lu, W., Yang, X., He, J., Le, X. et al. (2018). Bioinspired anisotropic hydrogel actuators with on-off switchable and color-tunable fluorescence behaviors. *Advanced Functional Materials*, 28(7), 1704568. DOI 10.1002/adfm.201704568.
37. Zhang, D., Ren, B., Zhang, Y., Xu, L., Huang, Q. et al. (2020). From design to applications of stimuli-responsive hydrogel strain sensors. *Journal of Materials Chemistry B*, 8(16), 3171–3191. DOI 10.1039/C9TB02692D.
38. Liu, H., Chen, X., Zheng, Y., Zhang, D., Zhao, Y. et al. (2021). Lightweight, superelastic, and hydrophobic polyimide nanofiber/mxene composite aerogel for wearable piezoresistive sensor and oil/water separation applications. *Advanced Functional Materials*, 372, 2008006. DOI 10.1002/adfm.202008006.

39. Hoffman, A. S. (2002). Hydrogels for biomedical applications. *Advanced Drug Delivery Reviews*, 54(1), 3–12. DOI 10.1016/S0169-409X(01)00239-3.
40. Shi, Y., Peng, L., Yu, G. (2015). Nanostructured conducting polymer hydrogels for energy storage applications. *Nanoscale*, 7(30), 12796–12806. DOI 10.1039/C5NR03403E.
41. Huang, Y., Zhong, M., Shi, F., Liu, X., Tang, Z. et al. (2017). An intrinsically stretchable and compressible supercapacitor containing a polyacrylamide hydrogel electrolyte. *Angewandte Chemie International Edition*, 56(31), 9141–9145. DOI 10.1002/anie.201705212.
42. Wang, M., Fan, L., Qin, G., Hu, X., Wang, Y. et al. (2020). Flexible and low temperature resistant semi-IPN network gel polymer electrolyte membrane and its application in supercapacitor. *Journal of Membrane Science*, 597, 117740. DOI 10.1016/j.memsci.2019.117740.
43. Ma, C., Gao, J., Wang, D., Yuan, Y., Wen, J. et al. (2019). Sunlight polymerization of poly(amidoxime) hydrogel membrane for enhanced uranium extraction from seawater. *Advanced Science*, 6, 1900085. DOI 10.1002/advs.201900085.
44. Wang, X., Su, M., Liu, C., Shen, C., Liu, X. (2020). Poly(vinyl alcohol)/graphene nanocomposite hydrogel scaffolds for control of cell adhesion. *Journal of Renewable Materials*, 8(1), 89–99. DOI 10.32604/jrm.2020.08493.
45. Hu, X.-S., Liang, R., Sun, G. (2018). Super-adsorbent hydrogel for removal of methylene blue dye from aqueous solution. *Journal of Materials Chemistry A*, 6(36), 17612–17624. DOI 10.1039/C8TA04722G.
46. Jv, X., Zhao, X., Ge, H., Sun, J., Li, H. et al. (2019). Fabrication of a magnetic poly(aspartic acid)-Poly(acrylic acid) hydrogel: Application for the adsorptive removal of organic dyes from aqueous solution. *Journal of Chemical & Engineering Data*, 64(3), 1228–1236. DOI 10.1021/acs.jced.8b01117.
47. Yang, Y., Wang, X., Yang, F., Wang, L., Wu, D. (2018). Highly elastic and ultratough hybrid ionic-covalent hydrogels with tunable structures and mechanics. *Advanced Materials*, 30(18), 1707071. DOI 10.1002/adma.201707071.
48. Xu, L., Wang, C., Cui, Y., Li, A., Qiao, Y. et al. (2019). Conjoined-network rendered stiff and tough hydrogels from biogenic molecules. *Science Advances*, 5(2), eaau3442. DOI 10.1126/sciadv.aau3442.
49. Zheng, S. Y., Yu, H. C., Yang, C., Hong, W., Zhu, F. et al. (2020). Fracture of tough and stiff metallosupramolecular hydrogels. *Materials Today Physics*, 13, 100202. DOI 10.1016/j.mtphys.2020.100202.
50. Wu, J., Li, P., Dong, C., Jiang, H., Bin, X. et al. (2018). Rationally designed synthetic protein hydrogels with predictable mechanical properties. *Nature Communications*, 9(1), 1352. DOI 10.1038/s41467-018-02917-6.
51. Shi, F. K., Zhong, M., Zhang, L. Q., Liu, X. Y., Xie, X. M. (2017). Toughening mechanism of nanocomposite physical hydrogels fabricated by a single gel network with dual crosslinking—The roles of the dual crosslinking points. *Chinese Journal of Polymer Science*, 35(1), 25–35. DOI 10.1007/s10118-017-1869-x.
52. Dragan, E. S., Lazar, M. M., Dinu, M. V., Doroftei, F. (2012). Macroporous composite IPN hydrogels based on poly(acrylamide) and chitosan with tuned swelling and sorption of cationic dyes. *Chemical Engineering Journal*, 204–206, 198–209. DOI 10.1016/j.cej.2012.07.126.
53. Dragan, E. S., Perju, M. M., Dinu, M. V. (2012). Preparation and characterization of IPN composite hydrogels based on polyacrylamide and chitosan and their interaction with ionic dyes. *Carbohydrate Polymers*, 88(1), 270–281. DOI 10.1016/j.carbpol.2011.12.002.
54. Farahani, B. V., Ghasemzadeh, H., Afraz, S. (2016). Intelligent semi-IPN chitosan-PEG–PAAm hydrogel for closed-loop insulin delivery and kinetic modeling. *RSC Advances*, 6(32), 26590–26598. DOI 10.1039/C5RA28188A.
55. Mahdavinia, G. R., Mousanezhad, S., Hosseinzadeh, H., Darvishi, F., Sabzi, M. (2016). Magnetic hydrogel beads based on PVA/sodium alginate/laponite RD and studying their BSA adsorption. *Carbohydrate Polymers*, 147, 379–391. DOI 10.1016/j.carbpol.2016.04.024.
56. Mohammed, N., Grishkewich, N., Waeijen, H. A., Berry, R. M., Tam, K. C. (2016). Continuous flow adsorption of methylene blue by cellulose nanocrystal-alginate hydrogel beads in fixed bed columns. *Carbohydrate Polymers*, 136(5), 1194–1202. DOI 10.1016/j.carbpol.2015.09.099.

57. Balakrishnan, B., Mohanty, M., Umashankar, P. R., Jayakrishnan, A. (2005). Evaluation of an in situ forming hydrogel wound dressing based on oxidized alginate and gelatin. *Biomaterials*, 26(32), 6335–6342. DOI 10.1016/j.biomaterials.2005.04.012.
58. Wei, Z., Yang, J. H., Liu, Z. Q., Xu, F., Zhou, J. X. et al. (2015). Novel biocompatible polysaccharide-based self-healing hydrogel. *Advanced Functional Materials*, 25(9), 1352–1359. DOI 10.1002/adfm.201401502.
59. Liang, H., Lu, Q., Liu, M., Ou, R., Wang, Q. et al. (2020). UV absorption, anticorrosion, and long-term antibacterial performance of vegetable oil based cationic waterborne polyurethanes enabled by amino acids. *Chemical Engineering Journal*, 127774. DOI 10.1016/j.cej.2020.127774.
60. Zhang, C., Liang, H., Liang, D., Lin, Z., Chen, Q. et al. (2020). Renewable castor-oil-based waterborne polyurethane networks: Simultaneously showing high strength, self-healing, processability and tunable multishape memory. *Angewandte Chemie International Edition*, 60(8), 4289–4299. DOI 10.1002/anie.202014299.
61. Wang, X., Liang, H., Jiang, J., Wang, Q., Luo, Y. et al. (2020). A cysteine derivative-enabled ultrafast thiol-ene reaction for scalable synthesis of a fully bio-based internal emulsifier for high-toughness waterborne polyurethanes. *Green Chemistry*, 22(17), 5722–5729. DOI 10.1039/D0GC02213F.
62. Liu, L., Lu, J., Zhang, Y., Liang, H., Liang, D. et al. (2019). Thermosetting polyurethanes prepared with the aid of a fully bio-based emulsifier with high bio-content, high solid content, and superior mechanical properties. *Green Chemistry*, 21(3), 526–537. DOI 10.1039/C8GC03560A.
63. Gombotz, W. R., Wee, S. F. (2012). Protein release from alginate matrices. *Advanced Drug Delivery Reviews*, 64(12), 194–205. DOI 10.1016/j.addr.2012.09.007.
64. Daemi, H., Barikani, M. (2012). Synthesis and characterization of calcium alginate nanoparticles, sodium homopolymannuronate salt and its calcium nanoparticles. *Scientia Iranica*, 19(6), 2023–2028. DOI 10.1016/j.scient.2012.10.005.
65. Kaşgöz, H., Özgümüş, S., Orbay, M. (2003). Modified polyacrylamide hydrogels and their application in removal of heavy metal ions. *Polymer*, 44(6), 1785–1793. DOI 10.1016/S0032-3861(03)00033-8.